

# Direct observation of the mass renormalization in $\text{SrVO}_3$ by angle resolved photoemission spectroscopy

T. Yoshida<sup>1</sup>, K. Tanaka<sup>1</sup>, H. Yagi<sup>1</sup>, A. Ino<sup>2</sup>, H. Eisaki<sup>3</sup>, A. Fujimori<sup>1</sup>, and Z.-X. Shen<sup>4</sup>

<sup>1</sup>*Department of Complexity Science and Engineering and Department of Physics,*

*University of Tokyo, Kashiwa, Chiba 277-8561, Japan*

<sup>2</sup>*Hiroshima Synchrotron Radiation Center, Hiroshima University,*

*Kagamiyama 2-313, Higashi-Hiroshima 739-8526, Japan*

<sup>3</sup>*National Institute of Advanced Industrial Science and Technology, Tsukuba 305-8568, Japan*

<sup>4</sup>*Department of Applied Physics and Stanford Synchrotron Radiation Laboratory, Stanford University, Stanford, CA94305*

(Dated: September 28, 2018)

We have performed an angle-resolved photoemission study of the three-dimensional perovskite-type  $\text{SrVO}_3$ . Observed spectral weight distribution of the coherent part in the momentum space shows cylindrical Fermi surfaces consisting of the V 3d  $t_{2g}$  orbitals as predicted by local-density-approximation (LDA) band-structure calculation. The observed energy dispersion shows a moderately enhanced effective mass compared to the LDA results, corresponding to the effective mass enhancement seen in the thermodynamic properties. Contributions from the bulk and surface electronic structures to the observed spectra are discussed based on model calculations.

PACS numbers: 71.18.+y, 71.20.-b, 71.27.+a, 71.30.+h, 79.60.-i

The effect of electron correlation on the electronic structure of the transition metal oxides (TMO) has been one of the most important and fundamental issues in condensed matter physics [1]. While the high- $T_c$  cuprates and the colossal magneto resistive (CMR) manganites belong to the charge-transfer regime of Zaanen-Allen-Sawatzky diagram [2], light transition-metal oxides such as perovskite-type Ti and V oxides are prototypical Mott-Hubbard-type systems. The metal-insulator transitions (MITs) in Ti and V oxides can be directly compared with theoretical predictions using the Hubbard model in, e.g. dynamical mean-field theory (DMFT), and are, therefore, ideal model systems to study electron correlation phenomena [3]. In earlier photoemission studies of perovskite-type Ti and V oxides, such as  $\text{Ca}_{1-x}\text{Sr}_x\text{VO}_3$  [4, 5] and  $\text{La}_{1-x}\text{Sr}_x\text{TiO}_3$  [6, 7], two characteristic structures in the transition-metal  $d$  band have been identified. One is the coherent part around the Fermi level ( $E_F$ ) corresponding to the band-like electronic structure, and the other is the incoherent part 1-2 eV away from  $E_F$  corresponding to the remnant of the lower Hubbard band (LHB), a behavior which is predicted by DMFT [8].

In the filling-control Mott-Hubbard system  $\text{La}_{1-x}\text{Sr}_x\text{TiO}_3$ , a critical mass enhancement toward the MIT has been observed in the electronic specific heats and magnetic susceptibility [9], analogous to the mass enhancement scenario developed by Brinkman and Rice [10]. A detail analysis of the coherent part of the photoemission spectra in  $\text{La}_{1-x}\text{Sr}_x\text{TiO}_3$  has revealed to some extent enhancement of the effective mass when approaching the MIT [7], which corresponds to the enhancement of the electronic specific heat coefficients  $\gamma$  toward the MIT critical point  $x \sim 0.06$ .

On the other hand,  $\text{Ca}_{1-x}\text{Sr}_x\text{VO}_3$  is a bandwidth-control Mott-Hubbard system. The photoemission re-

sults on  $\text{Ca}_{1-x}\text{Sr}_x\text{VO}_3$  have suggested that the transition from a correlated metal to the Mott insulating phase is characterized by spectral weight transfer from the coherent to the incoherent parts with decreasing  $x$  [4]. However, their  $\gamma$  does not show such a large change with  $x$  and no critical mass enhancement region is reached in this system [11]. Also, the width of the coherent part does not change appreciably with  $x$  while the photoemission spectral intensity at  $E_F$  increases as  $x$  increases. This behavior was interpreted due to a strong momentum dependence of the self-energy [4]. However, a recent “bulk-sensitive” photoemission study of  $\text{SrVO}_3$  and  $\text{CaVO}_3$  using soft X-rays indicated that the spectral weight of the coherent part is larger than that reported in the previous study with low photon energy and that there is no appreciable spectral weight transfer between  $\text{SrVO}_3$  and  $\text{CaVO}_3$  [12]. A photoemission study using several photon energies has indicated that the incoherent part includes a certain amount of contributions from the surface [13]. Theoretical studies have shown that the surface electronic structure should have a more strongly renormalized effective mass because of the reduced co-ordination number and hence the reduced bandwidth [14].

In order to address those fundamental unresolved issues, direct observation of band dispersion by angle-resolved photoemission spectroscopy (ARPES) would provide important information about the mass renormalization. In the present study, we have observed the band dispersion, the Fermi surface and hence the band renormalization in the three-dimensional Mott-Hubbard system  $\text{SrVO}_3$  by ARPES. Also, we shall address the issue of surface effects by obtained comparison of the spectra with the calculated bulk and surface electronic structures.

ARPES measurements were performed at Beamline 5-4 of Stanford Synchrotron Radiation Laboratory (SSRL)

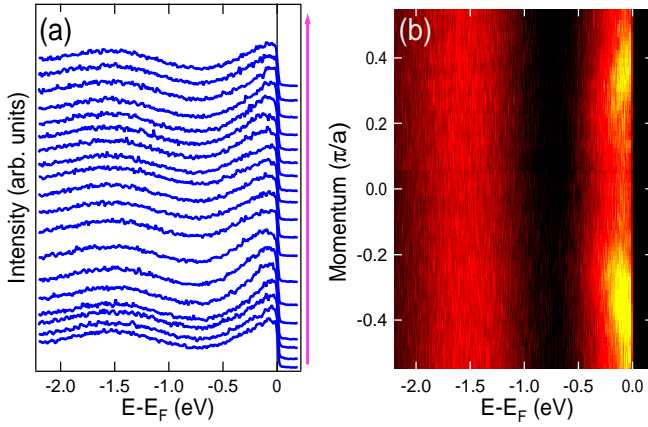


FIG. 1: ARPES spectra for SrVO<sub>3</sub> along momentum cut 4 in the Brillouin zone shown in Fig. 2. (a) EDC's. (b) Intensity plot in the  $E$ - $k_y$  plane. Dispersive feature within  $\sim 0.7$  eV of  $E_F$  is the coherent part, while broad feature around  $-1.5$  eV is the incoherent part.

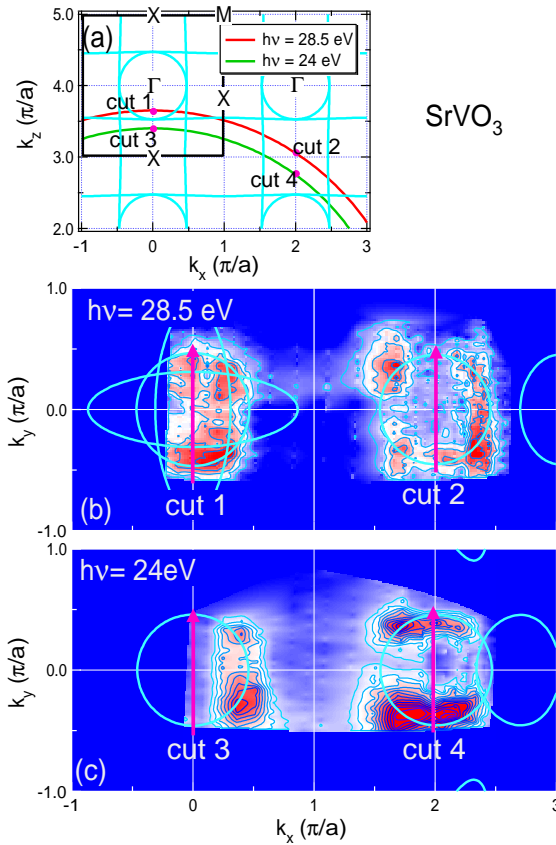


FIG. 2: Spectral weight mapping at  $E_F$ . (a)  $k_y=0$  cross-sectional view of the Fermi surfaces (blue curves) and the momentum loci corresponding to the mapping in panels (b) and (c). (b) Mapping for  $h\nu=28.5$  eV. (c) Mapping for  $h\nu=24$  eV. Note that the mapping is projection on the  $k_x$ - $k_y$  plane.

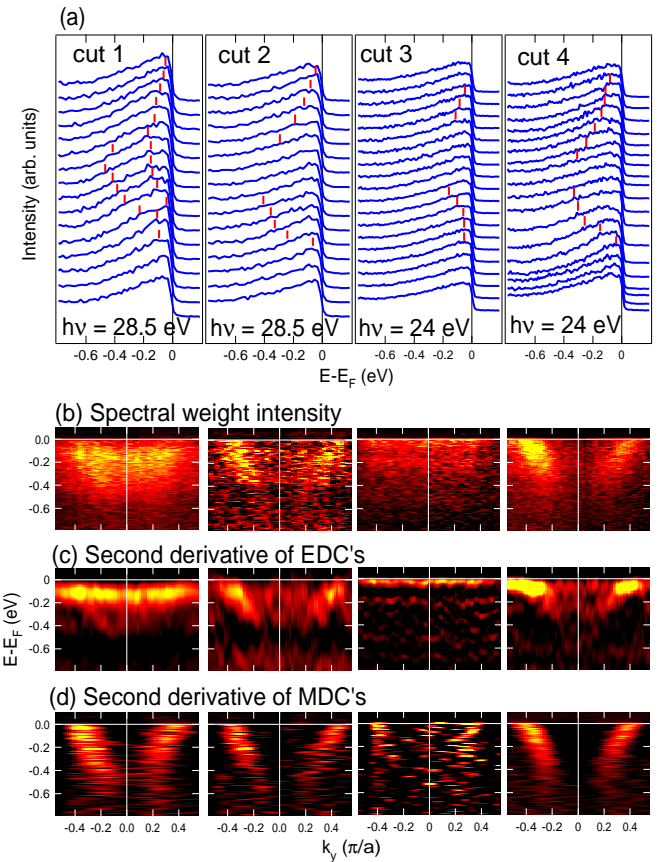


FIG. 3: (Color) Panels (a) show EDC's corresponding to the cuts in Fig. 2. Vertical bars are guides to the eyes indicating the positions of the dispersive features. Panels (b) are intensity plots in  $E$ - $k$  space of the EDC's in the panels (a). Angle-independent backgrounds have been subtracted. Second derivatives of the EDC's and MDC's are also shown in panels (c) and (d), respectively.

with a normal incidence monochromator and a Scienta SES-200 electron analyzer. The typical energy and angular resolutions used for the present measurements were about 30 meV and 0.3 degree, respectively. Single crystals of SrVO<sub>3</sub> were grown using the travelling-solvent floating zone method. Samples were first aligned by Laue diffraction *ex situ*, and cleaved along the cubic (100) surface and measured at a temperature of 15 K in a pressure better than  $5 \times 10^{-11}$  Torr. We have performed the measurements at photon energies  $h\nu=24$  and 28.5 eV. In this paper, the electron momentum is expressed in units of  $\pi/a$ , where  $a \sim 3.84$  Å, is the lattice constant corresponding to the V-O-V distance.  $k_x$  and  $k_y$  are the in-plane momenta and  $k_z$  are the out-of-plane ones.

First, we show an example of energy distribution curves (EDC's) for SrVO<sub>3</sub> in Fig. 1(a). The coherent part with  $\sim 0.7$  eV of  $E_F$  shows a dispersive feature, consistent with the view point that the coherent part corresponds to the band-structure calculation. On the other hand, the incoherent part centered at  $\sim -1.5$  eV does not show

a clear dispersion as seen in Fig 1(b). Background from angle-integrated spectra and the surface effects discussed below may hinder the observation of subtle dispersive features in the incoherent part. In the rest of this paper, we shall focus on the dispersive feature in the coherent part.

Figure 2 (a) illustrates the  $k_y=0$  cross-sectional view of the Fermi surfaces (blue curves) predicted by local-density approximation (LDA) band-calculation [15] and the loci of electron momenta in the  $k_x$ - $k_z$  plane for constant photon energies  $h\nu= 24$  eV and 28.5 eV. The inner potential of 10 eV has been assumed. Here, the LDA band-structure [15] to a tight-binding (TB) model consisting of three  $t_{2g}$  orbital  $d_{xy}$ ,  $d_{yz}$  and  $d_{zx}$  of V. The corresponding three bands do not hybridize with each other [16] within the present TB formalism which is the same as that in Ref. [14]. Figure 2 (b) and (c) shows spectral weight mapping in the  $k_x$ - $k_y$  momentum space at  $E_F$  on the momentum loci in panel (a) for the photon energies  $h\nu=28.5$  and 24 eV, respectively. Spectral weight is integrated over 30 meV within  $E_F$ . As seen in Fig. 2 (b) and (c), spectral weight for both photon energies are largely confined within the cylindrical Fermi surface extended in the  $k_z$  direction. According to panel (a), cuts 2 and 4 correspond to momenta near the X point [ $\mathbf{k} = (1, 0, 0)$ ]. Therefore, the observed spectral weight comes only from one cylindrical Fermi surface referred to as  $\gamma$  sheet [17] which arises from the  $d_{xy}$  orbital. On the other hand, the spectral weight in the first BZ for  $h\nu = 28.5$  eV (cut 1) is more intense than that for 24 eV (cut 3). This difference comes from the fact that the momentum locus for cut 1 is within the  $\alpha$ - and  $\beta$  sheets enclosed by the three cylindrical Fermi surfaces [17], while that for cut 3 is out of them. Indeed, energy distribution curves (EDC's) along cut 1 [Fig. 3 (a)] show complicated features suggestive of two energy dispersions.

Figure 3(a) shows EDC's along the four cuts in Fig. 2. Panels in Fig. 3(b) show spectral weight plots in the energy-momentum ( $E$ - $k$ ) space corresponding to each cut. The angle-independent EDC's have been subtracted as the background in these  $E$ - $k_y$  plots [18]. The second derivatives of the EDC's and the MDC's are shown in panels (c) and (d), respectively, so that one can visualize the band dispersions in spite of the high backgrounds. While cuts 2 and 4 show single energy dispersions, cut 1, which is around the  $\Gamma$  point, shows two band dispersions as in the EDC's in panel (a). This is due to the fact that the momenta of cut 1 are within the  $\alpha$  and  $\beta$  sheets of the Fermi surface.

In Fig. 4, we compare the  $E$ - $k_y$  plots with the energy dispersions expected from the LDA calculation. As seen in the EDC plots of cut 1 and cut 4 in Fig. 3, there are parabolic energy dispersions with the bottom at  $\sim -0.5$  eV, which is shallower than that expected from the LDA calculation  $\sim -0.9$  eV. The two dispersions observed for cut 1 in Fig. 3 may correspond to the dispersions of the

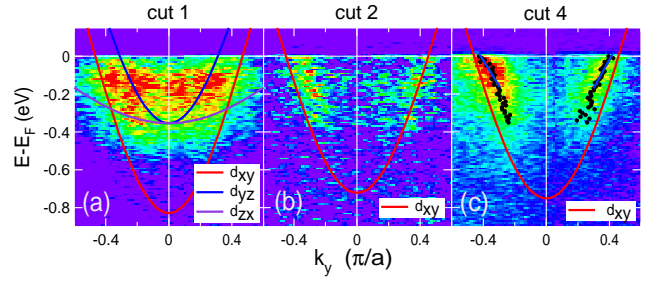


FIG. 4: (Color) Comparison of spectral weight distributions with calculated band dispersions. (a), (b) and (c) correspond to cuts 1, 2 and 4, respectively. Black dots in (c) are peak positions of MDC's and represents band dispersion.

$d_{xy}$  and  $d_{yz}$  bands, as shown in Fig. 4 (a). The dispersion of  $d_{zx}$  is not clearly observed in the present plot, probably due to the effect of transition matrix-elements. For cuts 2 and 4 [Fig. 4 (b) and (c)], since they do not intersect the  $d_{yz}$  and  $d_{zx}$  bands, we observed only the  $d_{xy}$  band.

In panel (c), we have derived the band dispersion for cut 4 from MDC peak positions indicated by black dots. By comparing the Fermi velocity of the LDA band structure and that of the present experiment, one can see the overall band narrowing in the measured band dispersion. Near  $E_F$ , we obtain the mass enhancement factor  $m^*/m_b \sim 1.8 \pm 0.2$ , which is close to the value  $m^*/m_b = 1.98$  obtained from the specific heat coefficient  $\gamma$  [11]. Since the LDA calculation predicted that the  $d_{xy}$  band is highly two-dimensional and isotropic within the  $k_x$ - $k_y$  plane, a similar mass enhancement is expected on the entire Fermi surface.

It has been pointed out that the photoemission spectra of this system taken at low photon energies have a significant amount of contributions from surface states, particularly in the incoherent part centered at  $\sim -1.5$  eV [12, 13]. In the photon energy range used in the present work, indeed, the bulk spectra has a smaller spectral weight compared to that of surface, by a factor of  $\sim 2$  [13]. However, surface spectra tend to have spectral weight in the incoherent part, reducing their spectral weight near  $E_F$ . Therefore, surface contributions are thought to be relatively small in the coherent part but may not be negligible. In order to distinguish bulk from surface contributions in the present spectra, we shall discuss the character of surface states.

Here, we consider several possible origins of surface states. One is a surface reconstruction, which may create two dimensional electronic states on the first layer different from bulk states. Such reconstruction-derived surface bands were observed in the ARPES spectra of  $\text{Sr}_2\text{RuO}_4$ . In that case, the surface band was symmetric with respect to the  $(\pi, 0)$ - $(0, \pi)$  line due to band folding into the new Brillouin zone of the  $\sqrt{2} \times \sqrt{2}$  superstructure. Since such a folded band has not been observed in the present results, the effect of surface reconstruc-

tion would not exist or would be negligible in the present ARPES spectra.

Another possible origin of surface states is the discontinuity of the potential at the surfaces. Figure 5 shows surface-projected density of states and band dispersion states calculated using a tight-binding Green's function formalism [19] for a semi-infinite system in the same manner as Ref. [14]. As shown in panels (a) and (b), the surface  $d_{xy}$  band does not show an appreciable change from the bulk band because it has the two-dimensional electronic structure within the  $x$ - $y$  plane. In contrast, spectral weight of the surface  $d_{yz,zx}$  states is redistributed between the bulk  $d_{yz,zx}$  band and the Fermi level [Fig. 5(c)], because  $k_z$  is no longer a good quantum number. This indicates that we cannot observe clear dispersions of the surface  $d_{yz,zx}$  bands in ARPES. Accordingly, the observed dispersion of the  $d_{xy}$  band should be similar to that of the bulk  $d_{xy}$  band and would therefore represent the bulk electronic states rather than the surface states.

In conclusion, we have directly observed the energy dispersions and the Fermi surfaces of SrVO<sub>3</sub> by ARPES. The observed effective mass renormalization in the  $d_{xy}$  band near  $E_F$  is consistent with the moderate mass enhancement in  $\gamma$ . From the model calculations of the surface electronic structure, we conclude that the observed dispersion of the  $d_{xy}$  band represents the bulk electronic structure. The present study has demonstrated that ARPES measurements are useful even for three-dimensional perovskite systems and provide direct information about the band renormalization in Mott-Hubbard system near MIT's.

We are grateful to M. Rozenberg and I. H. Inoue for enlightening discussions and D. H. Lu for technical support. This work was supported by a Grant-in-Aid for Scientific Research “Invention of Anomalous Quantum Materials” from the Ministry of Education, Science, Culture, Sports and Technology, Japan. SSRL is operated by the Department of Energy's Office of Basic Energy Science, Division of Chemical Sciences and Material Sciences.

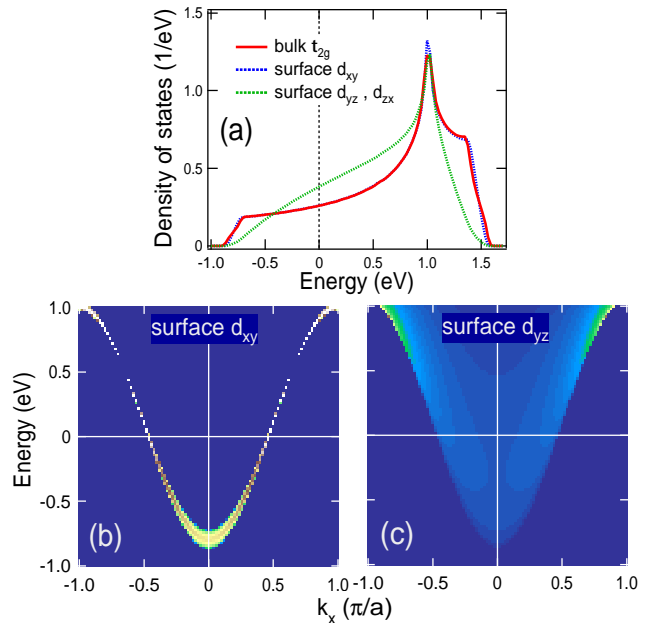


FIG. 5: Surface-projected electronic states calculated using the semi-infinite tight-binding model. (a) Density of states. (b) Spectral weight distribution of  $d_{xy}$  states. (c) Spectral weight distribution of  $d_{yz}$  states.

F. de Groot, Phys. Rev. Lett. **69**, 1796 (1992).

- [7] T. Yoshida, A. Ino, T. Mizokawa, A. Fujimori, Y. Taguchi, T. Katsufuji, and Y. Tokura, Europhys. Lett. **59**, 258 (2002).
- [8] A. Georges, G. Kotliar, W. Krauth, and M. J. Rozenberg, Rev. Mod. Phys. **68**, 13 (1996).
- [9] K. Kumagai, T. Suzuki, Y. Taguchi, Y. Okada, Y. Fujishima, and Y. Tokura, Phys. Rev. B **48**, 7636 (1993).
- [10] M. C. Gutzwiller, Phys. Rev. A **137**, A1726 (1965); W. F. Brinkmann and T. M. Rice, Phys. Rev. B **2** 4302 (1970).
- [11] I. H. Inoue, O. Goto, H. Makino, N. E. Hussey, and M. Ishikawa, Phys. Rev. B **58**, 4372 (1998).
- [12] A. Sekiyama, H. Fujiwara, S. Imada, S. Suga, H. Eisaki, S. I. Uchida, K. Takegahara, H. Harima, Y. Saitoh, I. A. Nekrasov, G. Keller, D. E. Kondakov, A. V. Kozhevnikov, Th. Pruschke, K. Held, D. Vollhardt, and V. I. Anisimov, Phys. Rev. Lett. **93**, 156402 (2004).
- [13] K. Maiti, P. Mahadevan, and D. D. Sarma, Phys. Rev. Lett. **80**, 2885 (1998).
- [14] A. Liebsch, Phys. Rev. Lett. **90**, 096401 (2003).
- [15] K. Takegahara, J. Elec. Spectrosc. Relat. Phenom. **66**, 303 (1994).
- [16] Distant-neighbor hopping causes hybridization between the three  $t_{2g}$  bands. However, this has small effect and may be a negligible in the present analysis.
- [17] I. H. Inoue, C. Bergemann, I. Hase, and S. R. Julian, Phys. Rev. Lett. **88**, 236403 (2002).
- [18] For the present analysis, we have used EDC's with no dispersive feature outside of the cylindrical Fermi surface as a background. The high background seen in the EDC's may come from the angle-integrated spectral weight due to disorder or imperfection of the irregularly cleaved or

fractured part of the surfaces. Nonetheless, we could observe clear structures with energy dispersions on the background. We consider that the dispersive features

come from the well cleaved part of the sample surface.  
[19] D. Kalkstein, P. Soven, *Surf. Science* **26**, 85 (1971).